LHC run 3, b-τ Yukawa unification, and dark matter implications in a SUSY 4-2-2 model

Waqas Ahmed,[1,*] Mohamed Belfkir,[2,†] Salah Nasri,[2,3,‡,§] Shabbar Raza,[4,‖] and Umer Zubair[5,¶]

[1]School of Mathematics and Physics, Hubei Polytechnic University, Huangshi 435003, China
[2]Department of Physics, United Arab Emirates University, Al Ain 15551 Abu Dhabi, UAE
[3]The Abdus Salam International Center for Theoretical Physics, Strada Costiera 11, I-34014 Trieste, Italy
[4]Department of Physics, Federal Urdu University of Arts, Science and Technology, Karachi 75300, Pakistan
[5]Division of Science and Engineering, Pennsylvania State University, Abington, Pennsylvania 19001, USA

(Received 7 January 2023; accepted 17 June 2023; published 13 July 2023)

We revisit the bottom and τ Yukawa coupling unification in the supersymmetric 4-2-2 model and present for the first time the sbottom-neutralino coannihilation scenario consistent with the bottom and τ Yukawa coupling unification. In addition, we present gluino-neutralino, stop-neutralino, stau-neutralino, chargino-neutralino, and A-resonance scenario and show that all such solutions are consistent with existing experimental collider constraints, *Planck* 2018 dark matter relic density bounds as well as direct and indirect bounds on neutralino-nucleons scattering cross sections. It is shown that in the sbottom-neutralino coannihilation scenario, the sbottom mass is between 1.2 to 3.5 TeV, whereas in the case of gluino-neutralino, stop-neutralino, the gluino mass can be between 1 to 3 TeV and the stop mass in the range of 1 to 3.5 TeV. Moreover, in the case of a coannihilation scenario, the stau and chargino masses can be as heavy as 3.5 TeV, while the A-resonance solutions are in the range of 0.5 to 3.5 TeV. We anticipate that some part of the parameter space will be accessible in the supersymmetry searches at LHC run 3 and beyond.

DOI: 10.1103/PhysRevD.108.015016

I. INTRODUCTION

The supersymmetric models possess several appealing features, such as the gauge coupling unification [1], resolution to the gauge hierarchy problem, and the potential for a dark matter candidate if augmented with R parity conservation [2]. It is worth mentioning that the minimal supersymmetric standard model (MSSM) predicts a Higgs boson of mass $m_h \lesssim 135$ GeV [3], whereas the observed Higgs boson mass at the Large Hadron Collider (LHC) is about 125 GeV [4,5]. Additionally, models such as supersymmetry (SUSY) $SO(10)$ and SUSY $SU(4)_C \times SU(2)_L \times SU(2)_R$ (4-2-2) can allow for the unification of the Yukawa couplings of the top quark, bottom quark, and tau lepton, known as t-b-τ or b-τ Yukawa unification (YU) [6–12]. (For a recent study in SUSY and non-SUSY frameworks, see [13,14]). In the SUSY 4-2-2 model, the soft supersymmetry breaking (SSB) mass terms for gauginos M_1, M_2, and M_3 corresponding to $U(1)_Y$, $SU(2)_L$, and $SU(3)_C$. The asymptotic MSSM gaugino masses can be nonuniversal in generic 4-2-2 models. This can be understood by considering C parity, which implies that the gaugino masses at $M_{\rm GUT}$ associated with $SU(2)_L$ and $SU(2)_R$ are equal. However, the asymptotic $SU(4)_C$ and consequently $SU(3)_C$ gaugino masses can differ. The hypercharge generator in 4-2-2 is given by $Y = \sqrt{\frac{2}{5}}(B-L) + \sqrt{\frac{3}{5}} I_{3R}$, where $B-L$ and I_{3R} are the diagonal generators of $SU(4)_C$ and $SU(2)_R$, respectively. As a result, we obtain the following asymptotic relation between the three MSSM gauginos

$$M_1 = \frac{3}{5} M_2 + \frac{2}{5} M_3. \tag{1}$$

The supersymmetric 4-2-2 model with C parity thus has two independent parameters (M_2, M_3) in the gaugino sector. This nonuniversality of gauginos along with the sign of Higgsino mass parameter μ can be utilized to explore very interesting phenomenology of the SUSY 4-2-2. Reference [12] showed the importance of $\mu < 0$ in achieving correct threshold corrections to the bottom quark Yukawa coupling and having light spectrum consistent with t-b-τ YU. It should be noted that the SUSY 4-2-2 is the only

*waqasmit@hbpu.edu.cn
†mohamed.belfkir@cern.ch
‡snasri@uaeu.ac.ae
§salah.nasri@cern.ch
‖shabbar.raza@fuuast.edu.pk
¶umer@udel.edu

model that yields gluino-neutralino coannihilation solutions consistent with dark matter relic density and 10% or better t-b-τ YU [9,11,15,16].

It was also shown in Refs. [9,11,15] that the t-b-τ YU in 4-2-2 model with the same sign SSB gaugino mass terms is consistent with lightest SUSY particle (LSP) neutralino dark matter through gluino-neutralino coannihilation channel. Moreover, for the combination $\mu < 0$ and gauginos with $M_2 < 0$ and $M_3 > 0$, it is shown that the solutions consistent with experimental constraints along with 10% or better t-b-τ YU can be realized in the 4-2-2 model for $m_0 \gtrsim 300$ GeV, as opposed to $m_0 \gtrsim 8$ TeV for the case of same sign gaugino masses, where m_0 represents the universal SSB mass parameter for scalars at $M_{\rm GUT}$ [12]. In this case, the coannihilation scenarios such as chargino-neutralino and stau-neutralino are available along with the A-funnel channel to achieve the correct dark relic density [12,17].

It is important to note that, in general, the t-b-τ YU is maintained in 4-2-2 model but not necessarily be kept intact if higher dimensional operators are also considered. In such a scenario, one can consider a set of higher dimensional operators whose contributions to the Yukawa couplings are expressed as $y_e/y_d = 1$ and $y_u/y_d \neq 1$ [18–20], such that one can still maintain the b-τ YU in 4-2-2 but not the t-b-τ YU.

In this paper, we update the status of b-τ YU in the line of the work reported in Ref. [21], in the light of LHC run 3 and new SUSY searches. In Ref. [21], t-b-τ YU and b-τ YU are considered with the same sign gaugino mass parameters and $\mu > 0$. In this study, it is shown that the coannihilation of next to lightest SUSY particle (NLSP) gluino, with the LSP neutralino, is the only channel available to obtain solutions consistent with experimental bounds and dark matter relic density bounds consistent with 10% or better t-b-τ YU. It should be noted that in such a scenario the heaviest NLSP gluino mass reported was about 1 TeV. In b-τ YU case, light stop NLSP coannihilation scenario with LSP neutralino was shown besides gluino-neutralino coannihilation where the NLSP gluino mass still remained around 1 TeV but the NLSP light stop mass was around 0.8 TeV. In a recent study [13] of t-b-τ YU in SUSY 4-2-2 with $\mu > 0$ but nonuniversal scalar mass parameters and gauginos with relative signs, it is shown that the NLSP gluino, NLSP stau and NLSP chargino coannihilation is possible with LSP neutralino and A-resonance solutions satisfying experimental constraints along with the dark matter relic density bounds and $R_{tb\tau} \lesssim 1.1$.

In this paper, we employ relative sign gaugino mass parameters and $\mu < 0$ and study sparticle spectrum consistent with collider bounds, 10% or better b-τ YU and dark matter relic density constraints in SUSY 4-2-2 framework. Since b-τ YU is a relaxed constraint as compared to t-b-τ YU, we expect a richer phenomenology. In fact, we do have very interesting phenomenological scenarios. For the first time we report the NLSP sbottom coannihilation with LSP neutralino scenario in SUSY 4-2-2 consistent with b-τ YU.[1] For sbottom-neutralino coannihilation with b-τ YU in $SU(5)$, see [23]. In Refs. [24,25] it was shown that the sbottom-neutralino coannihilation solutions consistent with experimental bounds were not compatible with b-τ YU in $SU(5)$. In fact, the NLSP sbottom coannihilation with the LSP neutralino requires nontrivial relationship among the SSB parameter. Besides, sbottom-neutralino coannihilation, we also have gluino-neutralino, stop-neutralino, stau-neutralino, chargino-neutralino, and A(H)-resonance solutions compatible with 10% or better b-τ YU and consistent with present experimental constraints. We show that our solutions are compatible with recent LHC SUSY searches, LHC run 3, and future projections. In addition, our solutions also satisfy dark matter constraints, such as *Planck* 2018 dark matter relic density bounds, dark matter direct and indirect current and future bounds.

The fundamental parameters of the 4-2-2 model under consideration are given as

$$m_0, m_{H_u}, m_{H_d}, A_0, M_2, M_3, \tan\beta, \mathrm{sign}(\mu). \tag{2}$$

Here m_0 is the universal SSB mass for MSSM sfermions, $m_{H_{u,d}}$ are Higgs SSB mass terms, A_0 is the universal terilinear scalar couplings, M_2 and M_3, as discussed before, are the gauginos SSB mass terms. M_1 is determined from M_2 and M_3, based on Eq. (1). All these parameters are defined at $M_{\rm GUT}$. The parameter $\tan\beta \equiv v_u/v_d$, which is the ratio of the vacuum expectation values of the two MSSM Higgs doublets, is defined at low scale.

The outline for the remainder of this paper is as follows. The summary of the scanning procedure and the experimental constraints employed in our analysis is given in Sec. II. We show results of scans for b-τ YU in Sec. III. We also provide a table of six benchmark points as an example of our results. Our conclusion is summarized in Sec. IV.

II. SCANNING PROCEDURE AND EXPERIMENTAL CONSTRAINTS

We use the ISAJET 7.85 package [26] to perform random scans on model parameters. In ISAJET, the unification condition at $M_{\rm GUT}$ is $g_U = g_1 = g_2$, and g_3 is allowed to deviate within 3%. We allow such deviation due to unknown threshold corrections at the GUT scale [27]. For a details discussion on the working of ISAJET package, see Ref. [26].

The fundamental parameters defined earlier are chosen in the following ranges:

[1]In fact, a couple of NLSP sbottom solutions also satisfy t-b-τ YU within 5%. In this article we are reporting the NLSP sbottom scenario and detailed study of such a scenario will be presented elsewhere [22].

$$\begin{aligned} 0\ \text{TeV} &\le m_0, m_{H_u}, m_{H_d} \le 20\ \text{TeV}, \\ -10\ \text{TeV} &\le M_2 \le 10\ \text{TeV}, \\ 0\ \text{TeV} &\le M_3 \le 5\ \text{TeV}, \\ 30 &\le \tan\beta \le 55, \\ -3 &\le A_0/m_0 \le 3, \end{aligned} \tag{3}$$

with $\mu < 0$ and $m_t = 173.3$ GeV [28].

We employ the Metropolis-Hastings algorithm in scanning the parameter space [29] and collect only those points which have successful radiative electroweak symmetry breaking (REWSB) and neutralino is the LSP to exclude solutions where the charged particles are stable [30,31]. Apart from these conditions, we also impose the mass bounds on all sparticles [32], and the constraints from rare decay processes: $B_s \to \mu^+\mu^-$ [33], $b \to s\gamma$ [34], and $B_u \to \tau\nu_\tau$ [35]. We also require LHC constraints on gluino and first/second generation squark masses [36] as well as the relic abundance of the LSP neutralino to satisfy the 5σ bounds of *Planck* 2018 data [37]. More explicitly, we set

$$m_h = (122\text{–}128)\ \text{GeV}, \tag{4}$$

$$m_{\tilde{g}} \ge 2.3\ \text{TeV}, \qquad m_{\tilde{q}} \ge 2\ \text{TeV}, \tag{5}$$

$$0.8 \times 10^{-9} \le \text{BR}(B_s \to \mu^+\mu^-) \le 6.2 \times 10^{-9}\ (2\sigma), \tag{6}$$

$$2.99 \times 10^{-4} \le \text{BR}(b \to s\gamma) \le 3.87 \times 10^{-4}\ (2\sigma), \tag{7}$$

$$0.15 \le \frac{\text{BR}(B_u \to \tau\nu_\tau)_{\text{MSSM}}}{\text{BR}(B_u \to \tau\nu_\tau)_{\text{SM}}} \le 2.41\ (3\sigma) \tag{8}$$

$$0.114 \le \Omega_{\text{CDM}}\, h^2(\text{Planck 2018}) \le 0.126\ (5\sigma). \tag{9}$$

Furthermore, we quantify b-τ YU with the parameter $R_{b\tau}$ defined as [29]

$$R_{tb\tau} \equiv \frac{\max(y_b, y_\tau)}{\min(y_b, y_\tau)}, \tag{10}$$

where $R_{b\tau} = 1$ implies perfect b-τ YU. However, we allow 10% ($R_{b\tau} = 1.1$) variation from the perfect unification due to various uncertainties.

III. RESULTS

A. Fundamental parameter space for b-τ YU

In this section we will discuss the impact of b-τ YU on the parameter space of the fundamental parameters of SUSY 4-2-2 model. In Figs. 1 and 2, the fundamental parameters are plotted against $R_{b\tau}$. The gray points are consistent with the REWSB and neutralino LSP conditions. The blue points represent sparticle mass bounds, Higgs mass bound, and B-physics bounds, whereas the red points satisfy 5σ Planck2018 bounds on the relic density of the LSP neutralino. The horizontal line shows the regions with $R_{b\tau} = 1.1$, below which lie the solutions with 10% or better b-τ YU.

The top left panel of Fig. 1 displays points in $m_0 - R_{b\tau}$ plane. It can be seen that as compared to $\mu > 0$ case, where one needs heavy universal scalar mass parameter, which is $7 \lesssim m_0 \lesssim 20$ TeV [21], we can have any value of m_0 between 0.5 to 20 TeV for opposite sign gauginos ($M_2 < 0$, $M_3 > 0$) with $\mu < 0$, consistent with 10% or better b-τ YU. This implies that we expect to have light to heavy spectrum with $R_{b\tau} \lesssim 1.1$. Similarly, points consistent with relic density bounds (red points) can be between 1 to 20 TeV. The concentration of red points in some regions is the result of focused scan. The top right panel of Fig. 1 shows solutions in the $A_0/m_0 - R_{b\tau}$ plane. We note that the solutions (both blue and red) consistent with $R_{b\tau} \lesssim 1.1$ can be anywhere between $-3 \lesssim A_0/m_0 \lesssim 3$. Here, again the concentration of more red points for $A_0/m_0 < 0$ is the result of more focused scans in this parameter space. The lower two panels of Fig. 1 show the parameters m_{H_d} (left) and m_{H_u} (right) plotted against $R_{b\tau}$. For m_{H_d}, the entire range of our scan satisfies 10% or better t-b-τ YU, whereas for m_{H_u}, the b-τ unification condition is satisfied only for $m_{H_d} \lesssim 11$ TeV.

Figure 2 shows the parameters M_2, M_3, and $\tan\beta$ plotted against $R_{b\tau}$. In the top left panel we see that there is no preferred value of M_2 for b-τ YU. We see that the solutions consistent with $R_{b\tau} \lesssim 1.1$ can be anywhere between -10 to 10 TeV. On the other hand, the plot in the top right corner shows that a gray region, $0\ \text{TeV} \lesssim M_3 \lesssim 1\ \text{TeV}$, is excluded because of the gluino mass bound. Except this gray region, the solutions consistent with $R_{b\tau}$ YU can be realized from 1 to 5 TeV. The lower panel shows that solutions satisfying 10% or better b-τ YU require $10 \lesssim \tan\beta \lesssim 60$.

B. Sparticle mass spectrum consistent with b-τ YU and dark matter constraints

In this section we display sparticle spectrum consistent with the b-τ YU, and other constraints discussed above including the dark matter relic density bounds.

Figure 3 displays the NLSP sbottom mass $m_{\tilde{b}_1}$ plotted against the LSP neutralino mass $m_{\tilde{\chi}_1^0}$ (left panel) and their mass difference $|\Delta m_{\tilde{\chi}_1^0, \tilde{b}_1}|$ (right panel). The set of gray points satisfy both the REWSB and LSP neutralino conditions, whereas the blue points satisfy the mass bounds and constraints from rare B-meson decays. On the other hand, the green points form a subset of blue points and satisfy $R_{b\tau} = 1.1$, whereas the red points are a subset of green points and are compatible with 5-σ *Planck* 2018 bounds on the relic density of the LSP neutralino. The diagonal line represents the coannihilation region where the NLSP sbottom is mass degenerate with the LSP neutralino. It is important to note that, in this paper, for the first time, the

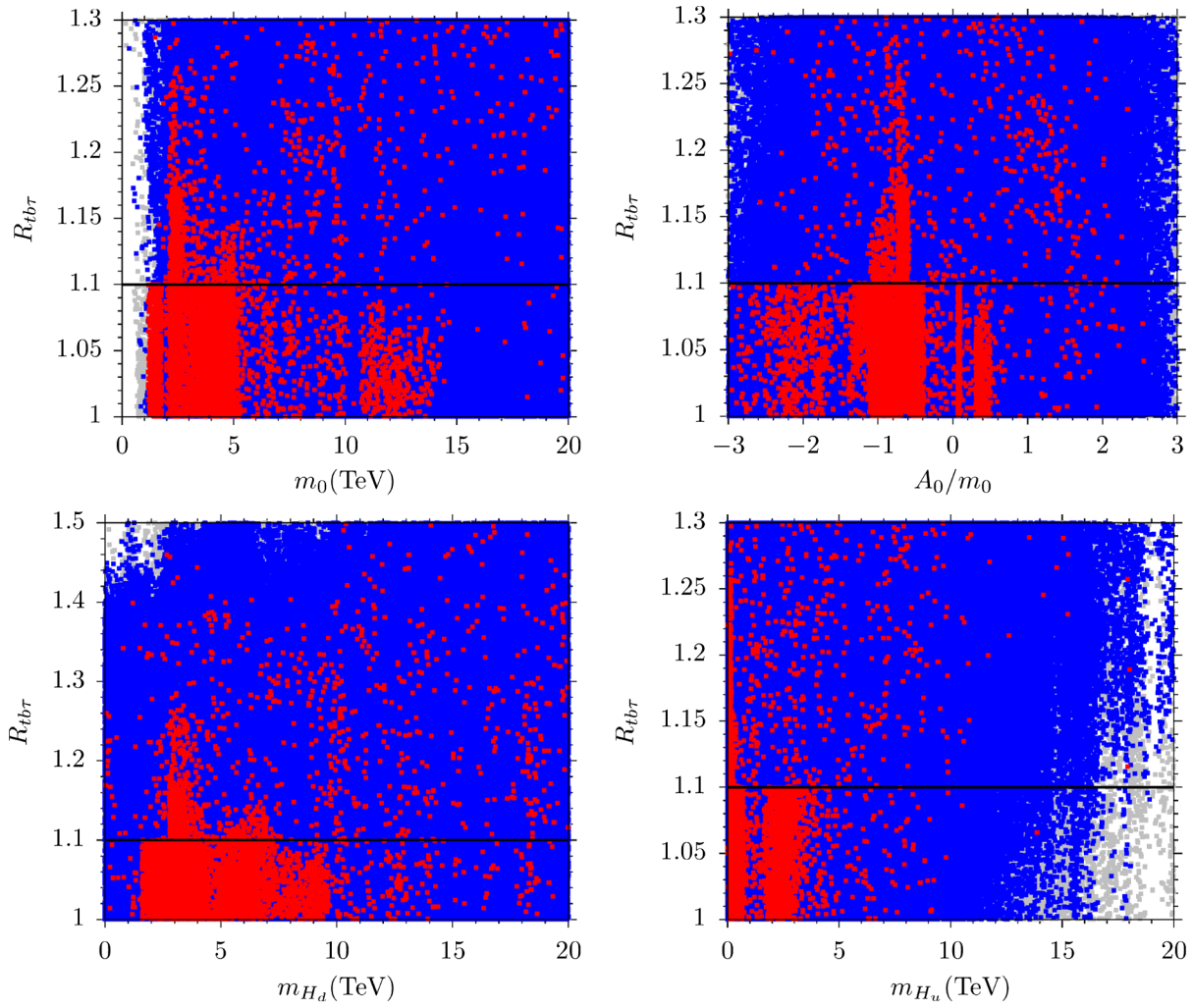

FIG. 1. Plots in the $m_0 - R_{b\tau}$, $A_0/m_0 - R_{b\tau}$, $m_{H_d} - R_{b\tau}$, and $m_{H_u} - R_{b\tau}$ planes. Gray points are consistent with the REWSB and LSP neutralino LSP conditions. Blue points represent sparticle mass bounds, Higgs mass bound, and B-physics bounds. Red points satisfy 5σ *Planck* 2018 bounds on the relic density of the LSP neutralino. The horizontal line shows the regions with $R_{b\tau} = 1.1$, below which are the solutions with 10% or better b-τ YU.

sbottom coannihilation parameter space is presented consistent with b-τ YU and other constraints in SUSY 4-2-2 model.[2] To the best of our knowledge, the sbottom-neutralino coannihilation parameter space consistent with b-τ YU has not been presented before in SUSY 4-2-2 model before. The detailed study of this scenario will be presented elsewhere [22]. The left panel of Fig. 3 shows that the NLSP sbottom solutions compatible with dark matter relic density bounds (red points) are between 1.2 to 3.5 TeV. Moreover, even if the relic density constraint is relaxed, the NLSP sbottom solutions (green points) also have more or less same mass ranges. Plot in the right panel of Fig. 3 shows the mass difference between NLSP sbottom and LSP neutralino as a function of NSLP sbottom mass. We would like to remind the readers that in this study we demand $\frac{\Delta m_{\rm NLSP,LSP}}{m_{\rm LSP}} \lesssim 10\%$, where $\Delta m_{\rm NLSP,LSP} = m_{\rm NLSP} - m_{\rm LSP}$. Therefore, the red points with small mass difference represent the sbottom NLSP solutions. We comment here in passing that if the mass difference is larger than the b quark mass, the available channel to search for NLSP sbottom is

$$pp \to \tilde{b}_1 \tilde{b}_1^* X \to b\bar{b} + \not{E}_{\rm inv}, \tag{11}$$

where $\tilde{b}_1 \to b\tilde{\chi}_1^0$.

There may also exist same sign sbottom pair productions $\tilde{b}_1\tilde{b}_1$ and $\tilde{b}_1^*\tilde{b}_1^*$. Recently there have been some searches for the light sbottom. For example, the ATLAS collaboration have shown that for $\tilde{b}_1 \to b\chi_2^0 \to bh\chi_1^0$ with $\Delta m_{\chi_1^0\chi_2^0} = 130$ GeV, sbottom mass can be ruled out up to 1.5 and 0.85 TeV [38,39], respectively. Similarly, for

[2]As we mentioned before, a couple of the NLSP sbottom solutions are also consistent with t-b-τ YU.

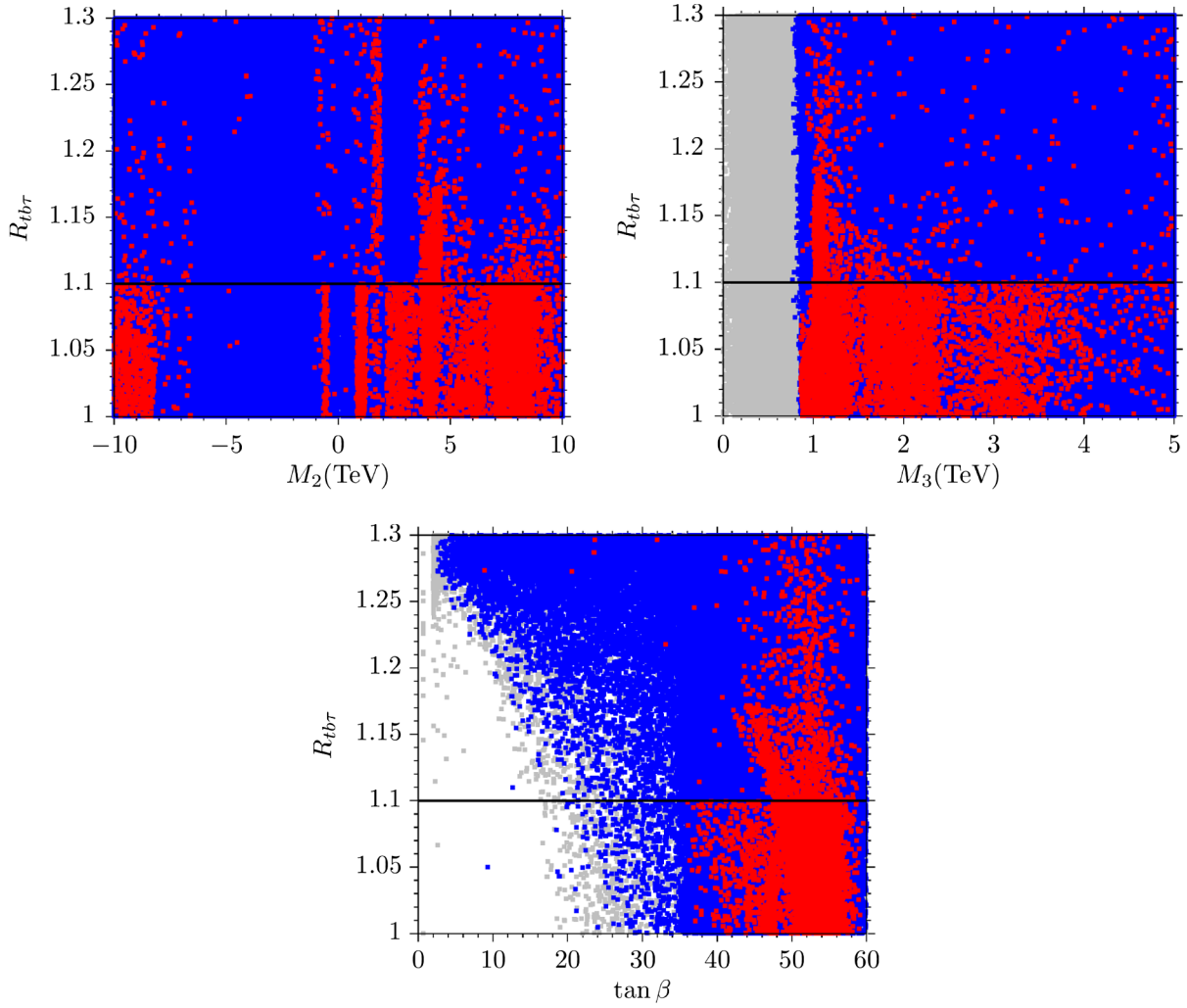

FIG. 2. Plots in the $M_2 - R_{b\tau}$ and $M_3 - R_{b\tau}$ and $\tan\beta - R_{b\tau}$, planes. The color coding is the same as in Fig. 1.

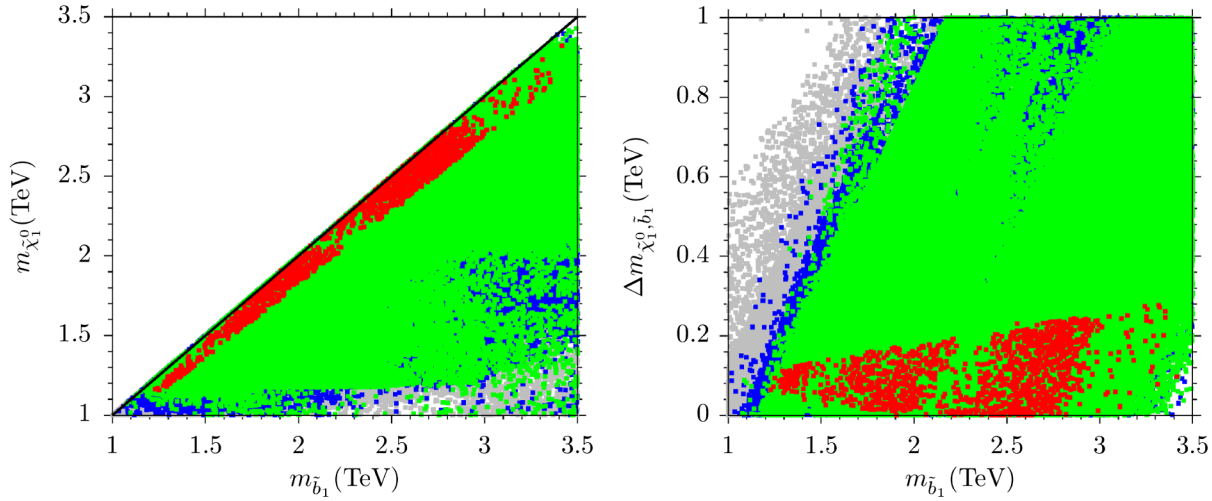

FIG. 3. Plots in the $m_{\tilde{b}_1} - m_{\tilde{\chi}_1^0}$ and $m_{\tilde{b}_1} - |\Delta m_{\tilde{\chi}_1^0,\tilde{b}_1}|$ planes. Gray points are compatible with the REWSB and LSP neutralino conditions. Blue points represent sparticle mass bounds, Higgs mass bound, and B-physics bounds. Green points form a subset of blue points and have $R_{b\tau} \lesssim 1.1$. Red points are a subset of green points, and they satisfy 5σ the *Planck* 2018 bound on the relic density of the LSP neutralino.

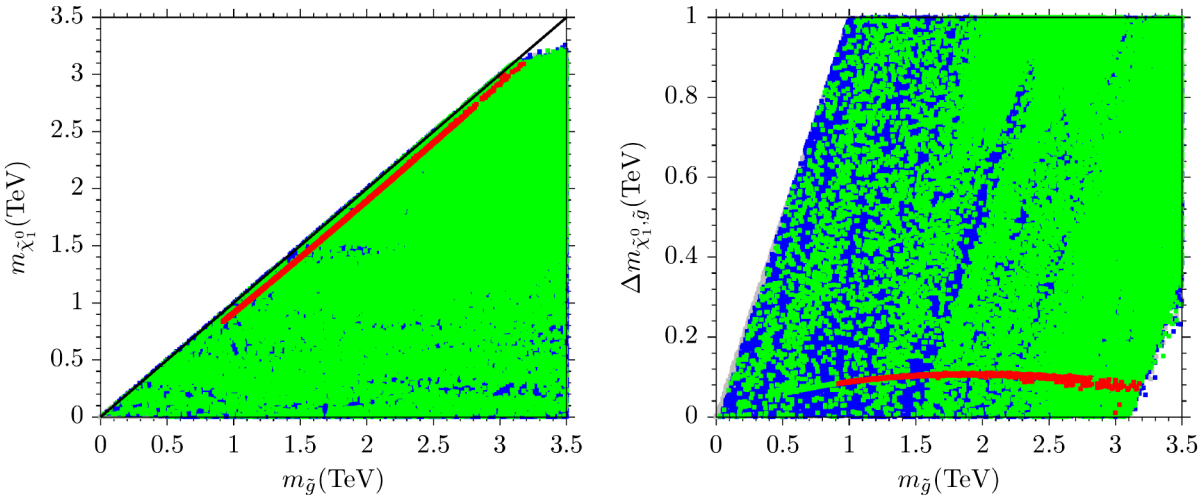

FIG. 4. Mass bounds and constraints in the $m_{\tilde{g}} - m_{\tilde{\chi}_1^0}$ and $m_{\tilde{g}} - |\Delta m_{\tilde{\chi}_1^0,\tilde{g}}|$ planes with same color scheme as in Fig. 3.

$\tilde{b}_1 \to t\chi_2^0$, with $\Delta m_{\chi_1^\pm,\chi_1^0} = 100$ GeV, the sbottom mass can be excluded up to 1.6 TeV [40]. Furthermore, for $\tilde{b}_1 \to b\chi_1^0$ (b-jets + $\not{E}$), NLSP sbottom can be excluded up to 1.270 TeV for massless neutralino. In case of $m_{\tilde{b}_1} \approx m_{\tilde{\chi}_1^0}$, one may employ dedicated secondary-vertex identification techniques to exclude $m_{\tilde{b}_1}$ up to 660 GeV for $\Delta m_{\tilde{b}_1,\tilde{\chi}_1^0} \sim 10$ GeV [41]. Similarly, for $\tilde{b}_1 \to b\chi_1^0$ (monojet) sbottom mass can be excluded up to 600 GeV. Also, according to [41], there is no mass limit on sbottom quark mass if it accedes to 800 GeV. It can be seen that in the first two cases, sbottom is not the NLSP but the last two channels are relevant, therefore our results are safe. We hope that in future collider searches, these solutions will be accessible to run 3.

Figure 4 shows the LSP neutralino mass $m_{\tilde{\chi}_1^0}$ (left panel) and their mass difference $|\Delta m_{\tilde{\chi}_1^0,\tilde{g}}|$ (right panel) plotted against the NLSP gluino mass $m_{\tilde{g}}$. Color coding is same as in Fig. 3, except we do not impose gluino mass bounds shown in Sec. II. It can be seen that the red points along the diagonal line fall between 0.8 to 3.2 TeV, which is a much better result compared to [21], where the NLSP gluino mass was around 1 TeV. In [13], the maximum reported NLSP gluino mass is 2.6 TeV, which is lower than ours. This is because they imposed the stricter condition of t-b-τ YU, while we only required b-τ YU, which is a more relaxed condition. Therefore, our higher NLSP gluino mass is understandable. In the right panel, the mass difference of gluino and neutralino ($\Delta m_{\tilde{g},\tilde{\chi}_1^0}$) as a function of gluino mass is shown. It is evident that the red points corresponding to the diagonal lines have $\Delta m_{\tilde{g},\tilde{\chi}_1^0}$ less than 100 GeV. In this scenario, the most dominant channel is $\tilde{g} \to b\bar{b}\chi_1^0$ as it provides the track jets, whereas the other decay channels will be suppressed by the high background contamination at low jet-p_T. Since we have a very compressed final state which means that the quarks will not have enough energy to

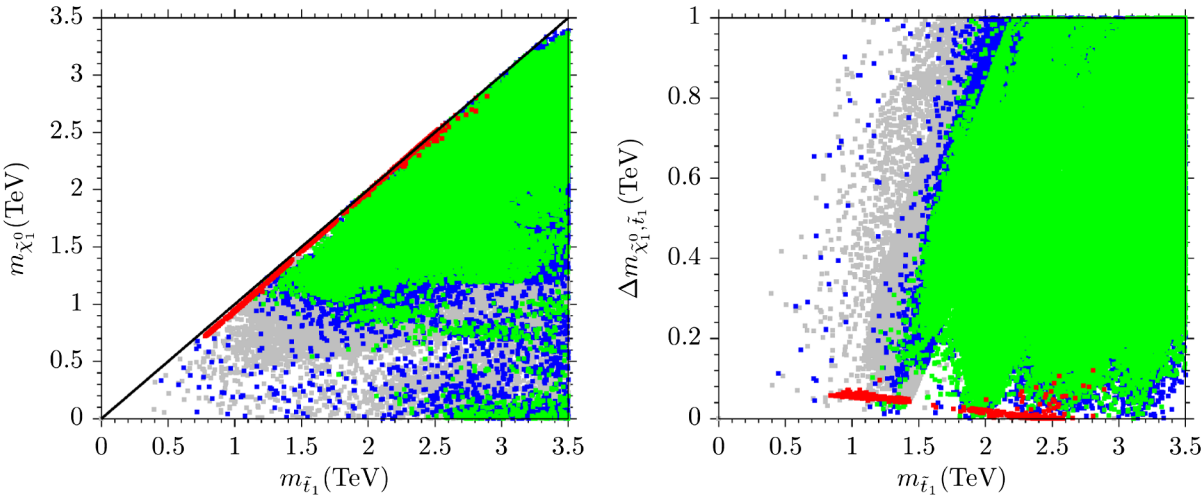

FIG. 5. Mass bounds and constraints in the $m_{\tilde{t}_1} - m_{\tilde{\chi}_1^0}$ and $m_{\tilde{t}_1} - |\Delta m_{\tilde{\chi}_1^0,\tilde{t}_1}|$ planes with same color scheme as in Fig. 3.

create tracks and hence the background will dominate for the case of light quarks, while with the b quark we have a secondary vertex and tracks that can still be reconstructed. In Refs. [42,43], one can extract mass limit on gluino mass in case of gluino-neutralino mass degenerate case which is about 1.2 TeV. This shows that our results are consistent with present searches but some solutions have already been excluded. A detailed collider analysis is needed to explore this scenario consistent with LHC run 3 and future colliders.

In the left panel of Fig. 5, the plot is shown in the $m_{\tilde{t}_1} - m_{\tilde{\chi}_1^0}$ plane. The color coding is the same as in Fig. 3. It should be noted that the NSLP stop solutions are present in b-τ YU scenarios but not in the t-b-τ YU case. Here, again, the NSLP stops solutions (red points) consistent with the 5σ dark matter relic density bounds along the black line. We see that, in our present scans, such NSLP stop solutions are spread in the interval of $\{0.9\text{–}2.9\}$ TeV. It is worth mentioning here that in Ref. [21], the NSLP stop solutions are up to 0.8 TeV. In previous studies of b-τ YU [25,44], the heaviest NSLP stop mass achieved was about 3 TeV. In our present study however, somehow we do not have a large density of green points in this region, therefore, there are no red points in the results. This is an artifact of scanning. Had we done some more focused scans, we would have populated this region of parameter space with more points and would have get NSLP stop solutions too. The right panel shows points in the $\Delta m_{\tilde{t}_1,\tilde{\chi}_1^0} - m_{\tilde{\chi}_1^0}$ plane. We note that, as compared to previous studies, for the red solutions, the difference between the NSLP light stop mass and the LSP neutralino can be as large as 120 GeV. This large mass difference corresponds to large stop and neutralino masses such that $\frac{\Delta m_{\rm NLSP,LSP}}{m_{\rm LSP}} \lesssim 10\%$ is still satisfied. Such a large mass difference kinematically allows decay channels, such as the three body decay $\tilde{t}_1 \to W + b + \tilde{\chi}_1^0$ and four body decay $\tilde{t}_1 \to f + f' + b + \tilde{\chi}_1^0$. On the other hand, for small mass difference, the above mentioned decay channels are kinematically not allowed but the loop induced two-body decay of NLSP stop, $\tilde{t}_1 \to c\chi_1^0$, is generally the dominant mode as compared to the four-body channel [45,46]. For previous studies, see [21], and for recent LHC studies, see [47–55]. In all of these studies, the maximum stop mass considered is 1.2 TeV as compared to our case where the minimum stop mass allowed by all constraints (red points) is about 800 GeV. Even for small mass gap where $\tilde{t}_1 \to c\tilde{\chi}_1^0$ dominates, the stop mass up to 550 GeV has been excluded [52]. It is evident the NLSP stop mass that we have shown here lies beyond these exclusion limits, but we hope that the future LHC searches will probe it.

Figure 6 shows various mass bounds and constraints in the $m_{\tilde{\tau}_1}$-$m_{\tilde{\chi}_1^0}$ (left) and $m_{\tilde{\tau}_1}$-$|\Delta m_{\tilde{\chi}_1^0,\tilde{\tau}}|$ (right) planes with the same color scheme as in Fig. 3. The left panel of Fig. 6 displays the stau-neutralino coannihilation, whereas the right panel shows the mass difference between stau and neutralino. It can be seen that in our scan, the light stau, degenerate in mass with neutralino, lies in the range $0.45\ \text{GeV} \lesssim m_{\tilde{\tau}_1} \lesssim 3.5$ TeV. Our results are therefore consistent with the results reported in [13,44]. Moreover, from Ref. [56] we note that our solutions are also consistent with the study published by CMS with 137 fb^{-1} at 13 TeV. We hope some of the parameter space we present here will be probed in LHC run 3 and beyond.

In addition to the coannihilation channels discussed above, our scans also yield charginio-neutralino coannihilation as shown in Fig. 7, where several constraints are displayed in the $m_{\tilde{\chi}_1^\pm}$-$m_{\tilde{\chi}_1^0}$ and $m_{\tilde{\chi}_1^\pm}$-$|\Delta m_{\tilde{\chi}_1^0,\tilde{\chi}_1^\pm}|$ planes. It can be seen that the red points, where the chargino is degenerate in mass with the LSP neutralino, are also consistent with b-τ YU in the mass range $0.3\ \text{TeV} \lesssim m_{\tilde{\chi}_1^\pm} \lesssim 3.5$ TeV. Our results are therefore consistent with [13]. Moreover, if we look at the recent searches for charginos, we note that for sleptons as well as SM-boson mediated decays of $\tilde{\chi}_1^+\tilde{\chi}_1^+$

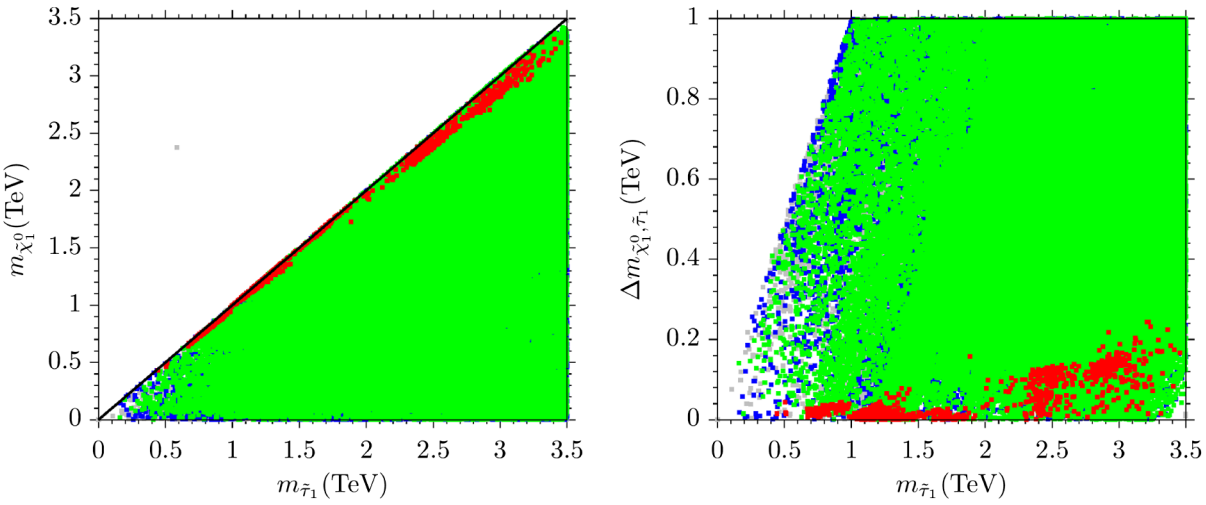

FIG. 6. Mass bounds and constraints in the $m_{\tilde{\tau}_1}$-$m_{\tilde{\chi}_1^0}$ and $m_{\tilde{\tau}_1}$-$|\Delta m_{\tilde{\chi}_1^0,\tilde{\tau}_1}|$ planes with same color scheme as in Fig. 3.

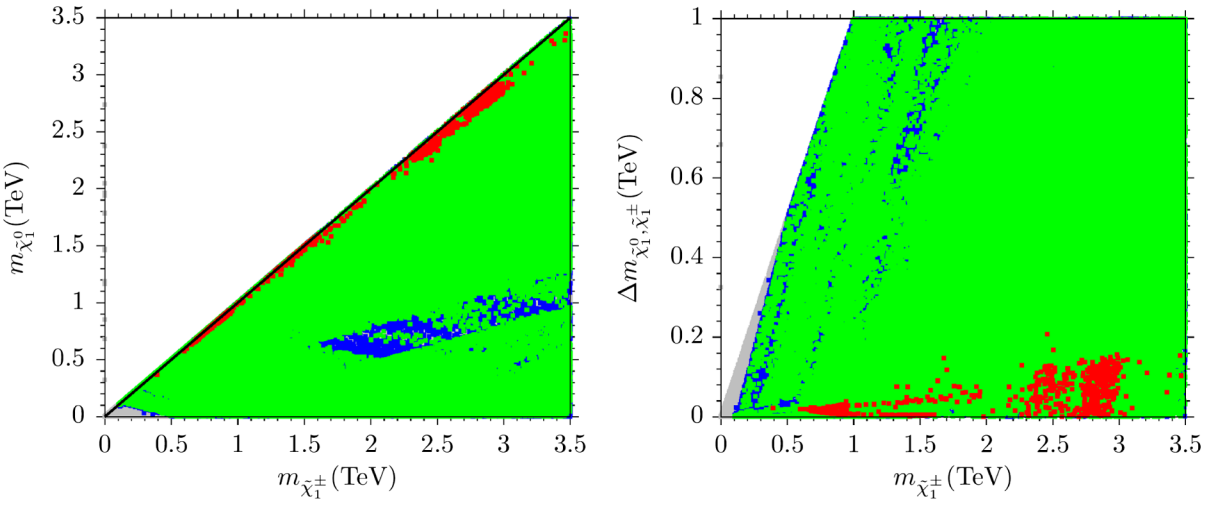

FIG. 7. Plots in the $m_{\tilde{\chi}_1^\pm}$-$m_{\tilde{\chi}_0^\pm}$ and $m_{\tilde{\chi}_1^\pm}$-$|\Delta m_{\tilde{\chi}_1^0,\tilde{\chi}_1^\pm}|$ planes. The color coding is the same as in Fig. 3.

and $\tilde{\chi}_1^\pm\tilde{\chi}_2^0$, the 95% exclusion limits are given in [43]. From this reference, we can see that if the charginos are degenerate with the LSP neutralino, solutions heavier than 300 GeV are safe. On the other hand in the parameter space where slepton masses are heavier than charginos, these slepton mediated decays will not take place. Since we also have heavier NLSP chargino solutions, we hope that such solutions will be probed in future LHC searches.

Besides the coannihilation channels we also have Higgs resonance scenario where a pair of LSP neutralinos decay via *CP*-odd (even) Higgs A (H,h) to SM particles. This may help in achieving the relic density in the allowed range. Figure 8 shows that it is possible to have solutions with $m_A \approx 2m_{\tilde{\chi}_1^0}$. We also note that in this scenario $m_A \sim m_H$. In Ref. [57], it is shown that for $A, H \to \tau\bar{\tau}$, $m_A \lesssim 1.7$ TeV is excluded for $\tan\beta \lesssim 30$. Similarly, it has been reported that for $\tan\beta \lesssim 10$ $m_A\sim$ can be excluded for the values 1, 1.1, and 1.4 TeV at run 2, run 3, and high luminosity LHC, respectively [58,59]. From our plots we see that the range of *A*-resonance solutions for neutralino mass lies between 0.4 and 3.5 TeV. Therefore, some part of the parameter space has already been explored by the LHC searches.

C. Dark matter implications

Finally, in this section we study the implications of b-τ YU and DM current and future searchers on the parameter space of 4-2-2. We note that, in the coannihilation and resonance scenarios we have discussed above, the LSP is a bino-type.

Figure 9 shows the spin-independent (SI) scattering cross section (left) and spin-dependent (SD) scattering cross section (right) of nucleons-neutralino as a function of the LSP neutralino mass. In the left panel, the solid black and yellow lines, respectively, represent the current LUX [60] and XENON1T [61] bounds, whereas the blue and brown lines depict the projection of future limits [62] of

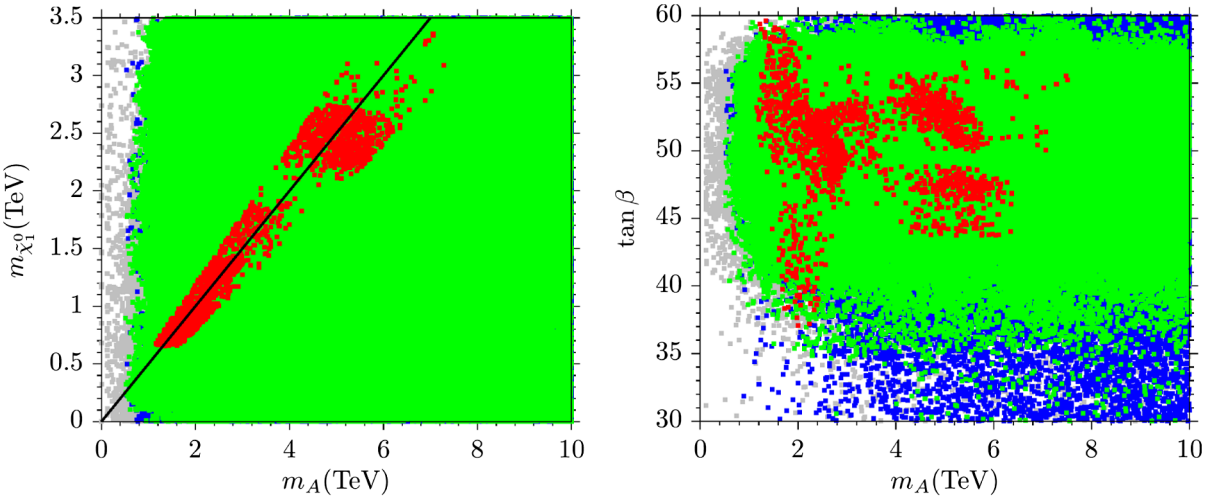

FIG. 8. Plots in the $m_A - m_{\tilde{\chi}_1^0}$ and $m_A - \tan\beta$ planes. The color coding is the same as in Fig. 3.

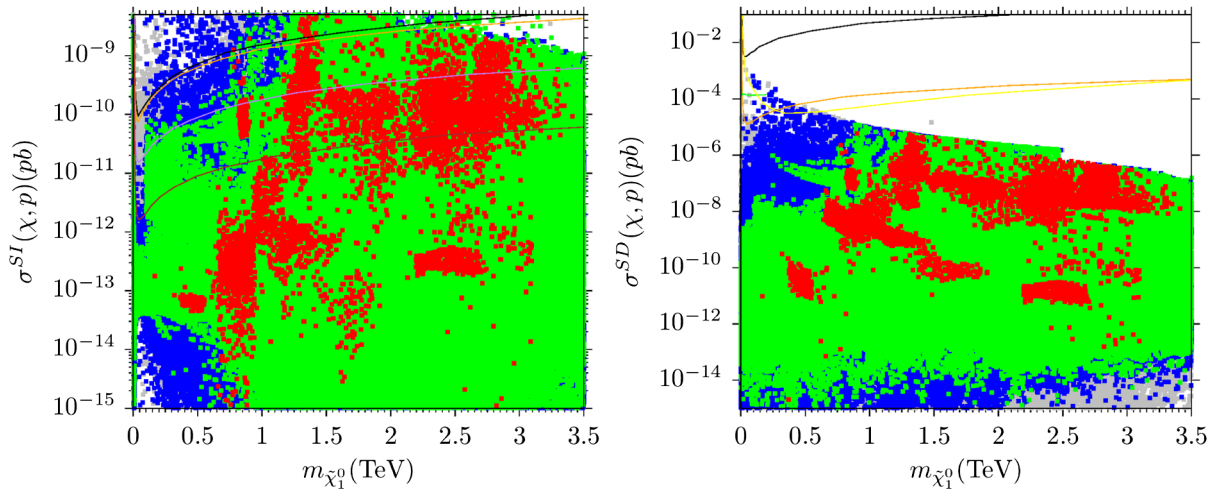

FIG. 9. Plots in the $m_{\tilde{\chi}_1^0} - \sigma^{SI}(\chi, p)(pb)$ and $m_{\tilde{\chi}_1^0} - \sigma^{SD}(\chi, p)(pb)$ planes. The color coding is the same as in Fig. 3.

TABLE I. Fundamental parameters and resulting sparticle mass spectrum of the 4-2-2 model. All masses are given in GeV.

	Point 1	Point 2	Point 3	Point 4	Point 5	Point 6
m_0	4979	6679	3426	2046	2357	2524
M_2	7491	7293	972.6	2535	2992	3049
M_3	1347	945.3	3033	1563	1002	1183
A_0/m_0	−0.4446	−0.9796	−0.8262	−1.243	−1.842	1.638
$\tan\beta$	55.5	55.1	52.15	54.77	46.5	49.73
m_{H_d}	5641	5979	4856	3333	2759	3652
m_{H_u}	337.4	1319	595.5	2683	2152	2774
m_h	**124**	**125**	**123**	**123**	**125**	**125**
m_H	3741	3925	3731	1318.28	1683.3	2116
m_A	3716	3899	3731	1309	1672	2102
$m_{H^\pm}$	3742	3926	3757	1322	1686	2118
$m_{\tilde{\chi}_{1,2}^0}$	2342, 2668	2236, 4805	800, 812	955, 1150	990, 1830	1037, 1424
$m_{\tilde{\chi}_{3,4}^0}$	2670, 6284	4807, 6183	4283, 4283	1150, 2109.	1835, 2503	1426, 2547
$m_{\tilde{\chi}_{1,2}^\pm}$	2582, 6240	4696, 6118	813, 4250	1105, 2079	1801, 2486	1386, 2525
$m_{\tilde{g}}$	3081	2329	6299.6	3378	2285	2652
$m_{\tilde{u}_{L,R}}$	7146, 5524	8178, 6868	6343, 6277	3837, 3532	3519, 3029	3821, 3358
$m_{\tilde{t}_{1,2}}$	3210, 5412	3929, 5975	5009, 5174	2165, 2741	1043, 2318	1361, 2507
$m_{\tilde{d}_{L,R}}$	7147, 5565	8179, 6919	6343, 6362	3837, 3533	3520, 3021	3822, 3358
$m_{\tilde{b}_{1,2}}$	2554, 5427	3821, 5968	4863, 5075	2226, 2728	1581, 2345	1803, 2535
$m_{\tilde{\nu}_{e,\mu}}$	6811	8055	3401	2607	3036	3178
$m_{\tilde{\nu}_\tau}$	6126	7169	2847	2188	2669	2713
$m_{\tilde{e}_{L,R}}$	6806, 5444	8051, 7011	3402, 3643	2608, 2234	3034, 2520	3177, 2712
$m_{\tilde{\tau}_{1,2}}$	3360, 6106	4646, 7151	2464, 2848	968, 2188	1434, 2662	1328, 2707
σ^{SI}(pb)	1.55×10^{-9}	1.0×10^{-12}	3.14×10^{-16}	2.93×10^{-10}	5.6×10^{-12}	7.66×10^{-10}
σ^{SD}(pb)	4.8×10^{-8}	1.75×10^{-10}	5.9×10^{-10}	8.3×10^{-7}	1.4×10^{-8}	1.39×10^{-7}
$\Omega_{\rm CDM}h^2$	0.120	0.1207	0.126	0.120	0.1175	0.124
$R_{b\tau}$	1.01	1.01062	1.001	1.0087	1.012	1.08

XENON1T with $2\,t\cdot y$ exposure and XENONnT with $20\,t\cdot y$ exposure, respectively. In the right panel, the black solid line represents the current LUX bound [63], the orange line represents the future Lux-Zeplin bound [64] and yellow line represents the IceCube DeepCore [65].

The plot in the $m_{\tilde{\chi}_1^0}$-σ^{SI} plane indicates that almost all of the red points meet the current experimental constraints for direct and indirect detection. However, some of the red points can be tested by the future XENON1T experiment with a $2\,t\cdot y$ exposure (dashed blue line), and almost half of the red solutions can be explored by the XENONnT experiment with a $20\,t\cdot y$ exposure (dashed brown line). This observation suggests that the dominant LSP neutralino is likely of bino-type, as the red solutions have relatively small neutralino-nucleon spin-independent scattering cross sections. Furthermore, the plot in the $m_{\tilde{\chi}^0}-\sigma^{SD}$ plane shows that our solutions align with the present and future potential of direct-detection experiments.

Finally, we show six benchmark points in Table I that summarize our findings for coannihilation scenarios. Point 1 is an example of NLSP-sbottom coannihilation where the NLSP sbottom is about 2.554 TeV with LSP neutralino (which is a bino of mass about 2.342 TeV) and b-τ YU is about 1%. We also note that in this case, the $\mathrm{BR}(\tilde{b}_1 \to b\tilde{\chi}_1^0)$ is 100%. Point 2 represents the NLSP gluino scenario where the gluino mass is about 2.329 TeV and the LSP neutralino (bino) has a mass of about 2.336 TeV with $R_{b\tau} = 1.01$, $\mathrm{BR}(\tilde{g} \to b\bar{b}\tilde{\chi}_1^0) = 0.6645$, and $\mathrm{BR}(\tilde{g} \to c\bar{c}\tilde{\chi}_1^0) = 0.1324$. Point 3 is an example of chargino-neutralino coannihilation, with $m_{\tilde{\chi}_1^0} = 0.813$ TeV, and a LSP neutralino, which is dominantly a bino with admixture of wino, that has mass around 0.8 TeV. Here $R_{b\tau} = 1.00$, $\mathrm{BR}(\tilde{\chi}_1^{\pm} \to q_i\bar{q}_i\tilde{\chi}_1^0)$ is about 33% ($i = u, d$ quarks), and $\mathrm{BR}(\tilde{\chi}_1^{\pm} \to l_i\bar{l}_i\tilde{\chi}_1^0)$ is about 11% ($i = e, \mu, \tau$ leptons). Point 4 represents a stau-neutralino coannihilation scenario. Here we see that NLSP stau mass is about 1.042 TeV, the LSP neutralino mass is about 0.990 TeV, and this is an example of 100% b-τ YU with $\mathrm{BR}(\tilde{\tau}_1 \to \tau\tilde{\chi}_1^0) = 1$. Similarly, point 5 depicts a stop-neutralino coannihilation scenario where the NLSP stop mass is about 1.042 TeV, LSP neutralino (bino) mass is about 0.990 TeV, $R_{b\tau} = 1.01$, and $\mathrm{BR}(\tilde{t}_1 \to c\tilde{\chi}_1^0)$ is 100%. It can be seen that, in point 6, m_A and m_H are almost degenerate and we can regard them either as a A- or H-resonance solution. For this point, the LSP bino mass is about 1.037 TeV, $m_A = 2.012$ TeV, and $m_H = 2.116$ TeV. Furthermore, the dominant branching fraction is $\mathrm{BR}(A/H \to b\bar{b}) = 0.8582$ and subdominant branching fraction is $\mathrm{BR}(A/H \to \tau\bar{\tau}) = 0.1352$ with $R_{b\tau} = 1.08$.

IV. CONCLUSION

In this article, we revisit the b-τ YU in the SUSY 4-2-2 model. We present, for the first time, the sbottom-neutralino coannihilation scenario that is consistent with b-τ YU and known experimental collider and astrophysical bounds. We also investigate gluino-neutralino, stop-neutralino, stau-neutralino, chargino-neutralino, and A-resonance scenarios and show that all of these solutions are consistent with existing experimental collider constraints, *Planck* 2018 dark matter relic density bounds, and direct and indirect bounds on neutralino-nucleon scattering cross sections. We demonstrate that in the sbottom-neutralino coannihilation scenario, the sbottom mass ranges from 1.2 to 3.5 TeV. In the gluino-neutralino and stop-neutralino cases, the gluino mass can be within the range of 0.8 to 3.2 TeV, and the stop mass can be between 0.8 to 3 TeV. Additionally, stau and chargino masses can reach up to 3.5 TeV in the coannihilation scenario, whereas the solutions associated with the A-resonance exhibit a neutralino mass range of 0.4 to 3.5 TeV. Finally, we anticipate that some parts of the parameter space will be assessable in the supersymmetry searches in LHC run 3 and future runs.

ACKNOWLEDGMENTS

The work of W. A. is partially supported by the Program for Excellent Talents in Hubei Polytechnic University (Grants No. 21xjz22R, No. 21xjz21R, and No. 21xjz20R). S. N. and M. B. are supported by the United Arab Emirates University (UAEU) under UAE Program for Advanced Research (UPAR) Grant No. 12S093. S. R. thanks Qaisar Shafi for introducing YU scenario in the SUSY 4-2-2 model.

[1] S. Dimopoulos, S. Raby, and F. Wilczek, Phys. Rev. D **24**, 1681 (1981); W. J. Marciano and G. Senjanovic, Phys. Rev. D **25**, 3092 (1982); U. Amaldi, W. de Boer, and H. Furstenau, Phys. Lett. B **260**, 447 (1991); J. R. Ellis, S. Kelley, and D. V. Nanopoulos, Phys. Lett. B **260**, 131 (1991); P. Langacker and M. X. Luo, Phys. Rev. D **44**, 817 (1991).

[2] G. Jungman, M. Kamionkowski, and K. Griest, Phys. Rep. **267**, 195 (1996).

[3] H. E. Haber and R. Hempfling, Phys. Rev. Lett. **66**, 1815 (1991); J. R. Ellis, G. Ridolfi, and F. Zwirner, Phys. Lett. B **257**, 83 (1991); Y. Okada, M. Yamaguchi, and T. Yanagida, Prog. Theor. Phys. **85**, 1 (1991); For a review, see e.g., M. S. Carena and H. E. Haber, Prog. Part. Nucl. Phys. **50**, 63 (2003).

[4] G. Aad *et al.* (ATLAS Collaboration), Phys. Lett. B **716**, 1 (2012).

[5] S. Chatrchyan *et al.* (CMS Collaboration), Phys. Lett. B **716**, 30 (2012).

[6] J. C. Pati and A. Salam, Phys. Rev. D **10**, 275 (1974); B. Ananthanarayan, G. Lazarides, and Q. Shafi, Phys. Rev. D **44**, 1613 (1991; Phys. Lett. B **300**, 24 (1993); Q. Shafi and B. Ananthanarayan, *Trieste HEP Cosmol.* (1991), pp. 233–244.

[7] See, incomplete list of references, L. J. Hall, R. Rattazzi, and U. Sarid, Phys. Rev. D **50**, 7048 (1994); B. Ananthanarayan, Q. Shafi, and X. Wang, Phys. Rev. D **50**, 5980 (1994); R. Rattazzi and U. Sarid, Phys. Rev. D **53**, 1553 (1996); T. Blazek, M. Carena, S. Raby, and C. Wagner, Phys. Rev. D **56**, 6919 (1997); J. L. Chkareuli and I. G. Gogoladze, Phys. Rev. D **58**, 055011 (1998); T. Blazek, S. Raby, and K. Tobe, Phys. Rev. D **62**, 055001 (2000); H. Baer, M. Brhlik, M. Diaz, J. Ferrandis, P. Mercadante, P. Quintana, and X. Tata, Phys. Rev. D **63**, 015007 (2001); C. Balazs and R. Dermisek, J. High Energy Phys. 06 (2003) 024; U. Chattopadhyay, A. Corsetti, and P. Nath, Phys. Rev. D **66**, 035003 (2002); T. Blazek, R. Dermisek, and S. Raby, Phys. Rev. Lett. **88**, 111804 (2002); M. Gomez, T. Ibrahim, P. Nath, and S. Skadhauge, Phys. Rev. D **72**, 095008 (2005); K. Tobe and J. D. Wells, Nucl. Phys. **B663**, 123 (2003); I. Gogoladze, Y. Mimura, and S. Nandi, Phys. Lett. B **562**, 307 (2003); W. Altmannshofer, D. Guadagnoli, S. Raby, and D. M. Straub, Phys. Lett. B **668**, 385 (2008); S. Antusch and M. Spinrath, Phys. Rev. D **78**, 075020 (2008); H. Baer, S. Kraml, and S. Sekmen, J. High Energy Phys. 09 (2009) 005; Phys. Rev. D **79**, 095004 (2009); K. Choi, D. Guadagnoli, S. H. Im, and C. B. Park, J. High Energy Phys. 10 (2010) 025; M. Badziak, M. Olechowski, and S. Pokorski, J. High Energy Phys. 08 (2011) 147; S. Antusch, L. Calibbi, V. Maurer, M. Monaco, and M. Spinrath, Phys. Rev. D **85**, 035025 (2012); J. S. Gainer, R. Huo, and C. E. M. Wagner, J. High Energy Phys. 03 (2012) 097; H. Baer, S. Raza, and Q. Shafi, Phys. Lett. B **712**, 250 (2012); I. Gogoladze, Q. Shafi, and C. S. Ün, J. High Energy Phys. 07 (2012) 055; M. Badziak, Mod. Phys. Lett. A **27**, 1230020 (2012); G. Elor, L. J. Hall, D. Pinner, and J. T. Ruderman, J. High Energy Phys. 10 (2012) 111; I. Gogoladze, Q. Shafi, and C. S. Un, Phys. Lett. B **704**, 201 (2011); I. Gogoladze, Q. Shafi, and C. S. Un, J. High Energy Phys. 08 (2012) 028; M. A. Ajaib, I. Gogoladze, and Q. Shafi, Phys. Rev. D **88**, 095019 (2013); M. Adeel Ajaib, I. Gogoladze, Q. Shafi, and C. S. Un, J. High Energy Phys. 07 (2013) 139; M. A. Ajaib, I. Gogoladze, Q. Shafi, and C. S. Un, arXiv:1308.4652.

[8] H. Baer, S. Kraml, S. Sekmen, and H. Summy, J. High Energy Phys. 03 (2008) 056; H. Baer, M. Haider, S. Kraml, S. Sekmen, and H. Summy, J. Cosmol. Astropart. Phys. 02 (2009) 002.

[9] I. Gogoladze, R. Khalid, and Q. Shafi, Phys. Rev. D **79**, 115004 (2009).

[10] H. Baer, S. Kraml, A. Lessa, and S. Sekmen, J. High Energy Phys. 02 (2010) 055.

[11] I. Gogoladze, R. Khalid, and Q. Shafi, Phys. Rev. D **80**, 095016 (2009).

[12] I. Gogoladze, R. Khalid, S. Raza, and Q. Shafi, J. High Energy Phys. 12 (2010) 055.

[13] M. E. Gómez, Q. Shafi, and C. S. Un, J. High Energy Phys. 07 (2020) 096.

[14] A. Djouadi, R. Fonseca, R. Ouyang, and M. Raidal, arXiv:2212.11315.

[15] S. Profumo and C. E. Yaguna, Phys. Rev. D **69**, 115009 (2004); D. Feldman, Z. Liu, and P. Nath, Phys. Rev. D **80**, 015007 (2009); N. Chen, D. Feldman, Z. Liu, P. Nath, and G. Peim, Phys. Rev. D **83**, 035005 (2011).

[16] M. A. Ajaib, T. Li, Q. Shafi, and K. Wang, J. High Energy Phys. 01 (2011) 028.

[17] I. Gogoladze, Q. Shafi, and C. S. Un, J. High Energy Phys. 07 (2012) 055.

[18] S. Antusch, S. F. King, and M. Spinrath, Phys. Rev. D **89**, 055027 (2014).

[19] S. Antusch and M. Spinrath, Phys. Rev. D **79**, 095004 (2009).

[20] S. Trine, S. Westhoff, and S. Wiesenfeldt, J. High Energy Phys. 08 (2009) 002.

[21] S. Raza, Q. Shafi, and C. S. Ün, Phys. Rev. D **92**, 055010 (2015).

[22] To be published.

[23] C. Pallis, Nucl. Phys. **B678**, 398 (2004).

[24] I. Gogoladze, S. Raza, and Q. Shafi, J. High Energy Phys. 03 (2012) 054.

[25] H. Baer, I. Gogoladze, A. Mustafayev, S. Raza, and Q. Shafi, J. High Energy Phys. 03 (2012) 047.

[26] H. Baer, F. E. Paige, S. D. Protopopescu, and X. Tata, arXiv:hep-ph/0001086.

[27] J. Hisano, H. Murayama, and T. Yanagida, Nucl. Phys. **B402**, 46 (1993); Y. Yamada, Z. Phys. C **60**, 83 (1993); J. L. Chkareuli and I. G. Gogoladze, Phys. Rev. D **58**, 055011 (1998).

[28] Tevatron Electroweak Working Group and CDF Collaboration and D0 Collaboration, arXiv:0903.2503.

[29] G. Belanger, F. Boudjema, A. Pukhov, and R. K. Singh, J. High Energy Phys. 11 (2009) 026; H. Baer, S. Kraml, S. Sekmen, and H. Summy, J. High Energy Phys. 03 (2008) 056.

[30] L. E. Ibanez and G. G. Ross, Phys. Lett. **110B**, 215 (1982); K. Inoue, A. Kakuto, H. Komatsu, and S. Takeshita, Prog. Theor. Phys. **68**, 927 (1982); **70**, 330(E) (1983); , **118B**, 73 (1982); J. R. Ellis, D. V. Nanopoulos, and K. Tamvakis, Phys. Lett. **121B**, 123 (1983); L. Alvarez-Gaume, J. Polchinski, and M. B. Wise, Nucl. Phys. **B221**, 495 (1983).

[31] J. Beringer *et al.* (Particle Data Group), Phys. Rev. D **86**, 010001 (2012).

[32] K. A. Olive *et al.* (Particle Data Group), Chin. Phys. C **38**, 090001 (2014).

[33] R. Aaij *et al.* (LHCb Collaboration), Phys. Rev. Lett. **110**, 021801 (2013).

[34] Y. Amhis *et al.* (Heavy Flavor Averaging Group), arXiv:1207.1158.

[35] D. Asner *et al.* (Heavy Flavor Averaging Group), arXiv:1010.1589.

[36] T. A. Vami (ATLAS and CMS Collaborations), *Proc. Sci.*, LHCP2019 (2019) 168 [arXiv:1909.11753].

[37] P. A. R. Ade *et al.* (Planck Collaboration), Astron. Astrophys. **594**, A13 (2016); Y. Akrami *et al.* (Planck Collaboration), arXiv:1807.06205.
[38] G. Aad *et al.* (ATLAS Collaboration), J. High Energy Phys. 12 (2019) 060.
[39] G. Aad *et al.* (ATLAS Collaboration), Phys. Rev. D **104**, 032014 (2021).
[40] G. Aad *et al.* (ATLAS Collaboration), J. High Energy Phys. 06 (2020) 046.
[41] G. Aad *et al.* (ATLAS Collaboration), J. High Energy Phys. 05 (2021) 093.
[42] ATLAS Collaboration, Report No. ATLAS-CONF-2018-041.
[43] ATLAS Collaboration, Report No. ATL-PHYS-PUB-2021-019.
[44] S. Raza, Q. Shafi, and C. S. Un, J. High Energy Phys. 05 (2019) 046.
[45] K. i. Hikasa and M. Kobayashi, Phys. Rev. D **36**, 724 (1987).
[46] M. Muhlleitner and E. Popenda, J. High Energy Phys. 04 (2011) 095.
[47] M. Aaboud *et al.* (ATLAS Collaboration), J. High Energy Phys. 12 (2017) 085.
[48] M. Aaboud *et al.* (ATLAS Collaboration), J. High Energy Phys. 06 (2018) 108.
[49] M. Aaboud *et al.* (ATLAS Collaboration), Eur. Phys. J. C **77**, 898 (2017).
[50] M. Aaboud *et al.* (ATLAS Collaboration), J. High Energy Phys. 01 (2018) 126.
[51] M. Aaboud *et al.* (ATLAS Collaboration), Eur. Phys. J. C **80**, 754 (2020).
[52] G. Aad *et al.* (ATLAS Collaboration), Phys. Rev. D **103**, 112006 (2021).
[53] G. Aad *et al.* (ATLAS Collaboration), Eur. Phys. J. C **80**, 737 (2020).
[54] G. Aad *et al.* (ATLAS Collaboration), J. High Energy Phys. 04 (2021) 174.
[55] G. Aad *et al.* (ATLAS Collaboration), J. High Energy Phys. 04 (2021) 165.
[56] CMS Collaboration, arXiv:2207.02254.
[57] CMS Collaboration, arXiv:2208.02717.
[58] H. Baer, V. Barger, X. Tata, and K. Zhang, Symmetry **14**, 2061 (2022).
[59] H. Baer, V. Barger, X. Tata, and K. Zhang, Symmetry **15**, 548 (2023).
[60] D. S. Akerib *et al.* (LUX Collaboration), Phys. Rev. Lett. **118**, 021303 (2017).
[61] E. Aprile *et al.* (XENON Collaboration), Phys. Rev. Lett. **119**, 181301 (2017); E. Aprile *et al.* (XENON Collaboration), Phys. Rev. Lett. **121**, 111302 (2018).
[62] E. Aprile *et al.* (XENON Collaboration), J. Cosmol. Astropart. Phys. 04 (2016) 027.
[63] D. S. Akerib *et al.* (LUX Collaboration), Phys. Rev. Lett. **118**, 251302 (2017).
[64] D. S. Akerib *et al.* (LUX Collaboration), Phys. Rev. Lett. **116**, 161302 (2016).
[65] R. Abbasi *et al.* (IceCube Collaboration), Phys. Rev. Lett. **102**, 201302 (2009).